Some Observational Evidence for Dry Soils Supporting Enhanced Relative Humidity at the Convective Boundary Layer Top

D. WESTRA, G. J. STEENEVELD, AND A. A. M. HOLTSLAG

Meteorology and Air Quality Section, Wageningen University, Wageningen, Netherlands

(Manuscript received 18 October 2011, in final form 16 April 2012)

ABSTRACT

The tendency of the relative humidity at the top of a clear convective boundary layer (RH_{top}) is studied as an indicator of cloud formation over a semiarid region within the conceptual framework introduced by Ek and Holtslag. Typically the tendency of RH_{top} increases if the evaporative fraction at the land surface increases, which supports boundary layer moistening but only when boundary layer growth is limited by atmospheric factors. This regime was supported by Cabauw observations in the original study. Here, new observational evidence that the tendency of RH_{top} can also increase as the surface becomes more dry, as is consistent with another regime of the conceptual framework, is provided. The observations used are from the African Monsoon Multidisciplinary Analyses (AMMA) intensive observational campaign near Niamey, Niger, 20–25 June 2006. In addition, the authors evaluate whether various versions of the Weather Research and Forecasting single-column model confirm the different regimes of the conceptual framework for a typical day in the AMMA campaign. It appears that the model confirms that dryer soils can support cloud formation.

1. Introduction

The physical mechanisms behind cumulus convection have been intensively studied for many regions all over the world (e.g., Wilde et al. 1985; Wetzel 1990; Ek and Mahrt 1994; Schlemmer et al. 2010, 2011). Despite these research efforts, onset of cumulus convection remains a challenge to forecast in numerical weather prediction (NWP) and climate models (e.g., Guichard et al. 2004; N. M. Taylor et al. 2011). Overall, models have difficulty representing gradual cloud growth (Bechtold et al. 2004; Rio et al. 2009) and the diurnal cycle of convective precipitation (e.g., Betts and Jakob 2002). Physically speaking, the land–atmosphere processes play a crucial role in cumulus onset; that is, surface evaporation and the consequent moisture availability at the top of the atmospheric boundary layer (ABL) are key to cumulus formation.

In semiarid regions, cumulus clouds may develop into mesoscale convective systems (MCSs). These MCSs are largely triggered by the state of the land–atmosphere system—that is, the soil moisture and boundary layer humidity content. Moreover, spatial heterogeneity such as topography, temperature, and moisture differences are relevant to MCS development as well (Comer et al. 2007). Climatologically, 88% of the total rainfall in the Sahel originates from MCSs. Hence, it is important to correctly forecast cumulus formation and to understand its physics. Therefore, the African Monsoon Multidisciplinary Analyses (AMMA) measurement campaign in the semiarid region such as the Sahel was established (Redelsperger et al. 2006). Ever since, many studies have reported on shallow cumulus onset and the transition to deep convection over this particular area (e.g., Couvreux et al. 2012; Lothon et al. 2011; C. M. Taylor et al. 2011).

In this paper the AMMA observations (Redelsperger et al. 2006) are used to evaluate the conceptual modeling framework by Ek and Holtslag (2004, hereafter EH04) for dry surface conditions. Interestingly and somewhat counterintuitively, tendency of the RH_{top} was found to *increase* with *decreasing* soil moisture content (w) for sufficiently weak free atmospheric stability. In such cases the ABL can grow deep such that the lifting condensation level (LCL) is lower than the ABL depth, supporting low-level cloud formation. We will refer to this regime as the "dry soil RH increase" (DSRHI) regime. Note that to avoid confusion, we wish to emphasize that we do not study cloud formation itself, but focus on the RH tendency at the ABL top, which is an indicator for boundary layer clouds.

Corresponding author address: G. J. Steeneveld, P.O. Box 47, 6700 AA Wageningen, Netherlands.
E-mail: gert-jan.steeneveld@wur.nl

DOI: 10.1175/JHM-D-11-0136.1

Our specific goal is to explore the observational evidence for the DSRHI regime. So far the DSRHI regime was only implied by the EH04 modeling framework, and observational support for this regime has been lacking. Thus, first the hypothesis of the DSRHI regime will be evaluated from AMMA field data. Second, we evaluate the Weather Research and Forecasting (WRF) single-column model against AMMA observations for four alternative ABL schemes [the first-order closure schemes Yonsei University (YSU) and Medium-Range Forecast (MRF), and the 1.5-order closure schemes Mellor–Yamada–Janjić (MYJ) and Quasi-Normal Scale Elimination (QNSE)] and the Noah land surface model (LSM), to examine which scheme performs best for the clear ABL in this particular region and whether WRF can reproduce the DSRHI regime.

The paper is organized as follows. Section 2 discusses briefly the relevant land–atmosphere interactions, section 3 summarizes the utilized methods and observations, and section 4 presents the results and discussion. Finally, conclusions are drawn in section 5.

2. Land–atmosphere coupling and cumulus onset

The coupling between the land surface and ABL plays a key role in cumulus onset and has been studied intensively (Jacobs and De Bruin 1992; Ek and Mahrt 1994; Santanello et al. 2005, 2007; van Heerwaarden et al. 2009; N. M. Taylor et al. 2011). EH04 found that cumulus onset may not only occur in relatively moist regimes but also in the DSRHI regime. To understand the process of cumulus onset in the latter regime, it is instructive to review the role of land–atmosphere interactions in cumulus onset over dry regions.

In midlatitude environments, under constant net radiation, a larger latent heat flux (LE) leads to a decrease of sensible heat flux (H) and therefore smaller ABL depths (h). Consequently, larger LE leads both directly and indirectly to moistening of the ABL. However, a more humid ABL does not automatically lead to cumulus onset when the lifting condensation level is not reached. On the other hand, in semiarid regions the soil is rather dry in the early stage of the monsoon. Therefore, LE is very low, H is relatively high, and the ABL becomes relatively deep. The low LE promotes drying of the ABL both directly and indirectly. Intuitively, one would expect that cumulus onset is unlikely in this regime. However, for ABL growth also the upper air stability is important (Haiden 1997; EH04). For a fairly weak free atmospheric stability (γ_θ), ABL top entrainment and growth are promoted. As the LCL in these regimes is found at higher altitudes, one expects that the LCL can only be reached if upper-level stability is sufficiently weak (see EH04). The increasing ABL height invokes a lower temperature at the ABL top, which decreases the saturation specific humidity (q_{sat}) and increases RH_{top} (Ek and Mahrt 1994). Consequently, as the ABL top crosses the LCL, cumulus onset becomes more plausible, even over dry regions.

Next, we briefly summarize the conceptual framework of EH04 to study the relative impact of surface and atmospheric forcings in the onset of cumulus clouds. This conceptual framework predicts the RH tendency on the basis of the available energy at the surface, atmospheric forcings (denoted below by ne), and the evaporative fraction (ef).

At the top of a convective boundary layer, the RH tendency is given by (see EH04 for details and derivation)

$$\frac{d\text{RH}_{\text{top}}}{dt} = \left(\frac{Q^* - G}{\rho L_v h q_{\text{sat,top}}}\right)[\text{ef} + \text{ne}(1 - \text{ef})]. \quad (1)$$

In the derivation of Eq. (1) the mixed-layer equations for the ABL (e.g., Deardorff 1979; Driedonks and Tennekes 1984) are utilized. The term on the left-hand side represents the RH tendency, Q^* represents the net radiation, G the soil heat flux, ρ is the air density, L_v is the latent heat of vaporization, and $q_{\text{sat,top}}$ is the saturation specific humidity at the ABL top. These variables represent the available energy term of the equation. The evaporative fraction (ef) and the nonevaporative terms (ne) are given by (EH04)

$$\text{ef} = \frac{LE}{H + LE} \quad (2)$$

and

$$\text{ne} = \frac{L_v}{c_p}(1 + C_\theta)\left[\frac{\Delta q}{h\gamma_\theta} + \text{RH}_{\text{top}}\left(\frac{c_2}{\gamma_\theta} - c_1\right)\right]. \quad (3)$$

It is directly clear that ef is solely determined by surface processes—that is, both sensible (H) and latent heat (LE). The atmospheric (nonevaporative) term is determined by the latent heat of water vapor (L_v), specific heat of dry air (c_p), the magnitude of the entrainment ratio at the ABL top ($C_\theta = 0.2$ in this study), the specific humidity discontinuity (Δq) at the ABL top, the ABL height, and the potential temperature lapse rate and the RH. The three terms in Eq. (3) can be physically interpreted as ABL dry air entrainment ($\Delta q/h\gamma_\theta$), boundary layer growth ($\text{RH}_{\text{top}}c_2/\gamma_\theta$), and boundary layer heating due to surface warming and warm air entrainment ($\text{RH}_{\text{top}}c_1$). Finally, factors c_1 and c_2 are determined by the pressure at the ABL top and temperature as follows:

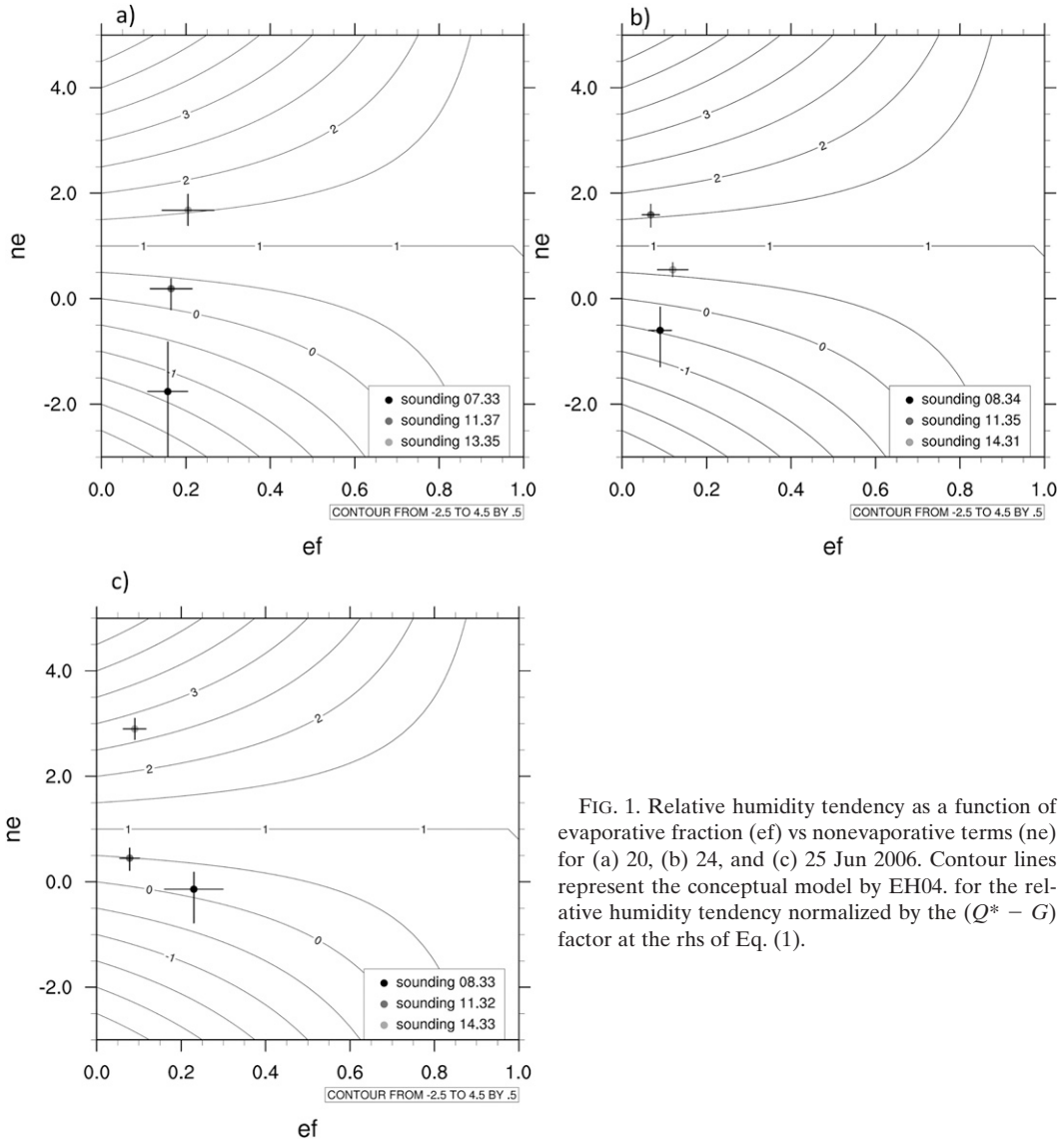

FIG. 1. Relative humidity tendency as a function of evaporative fraction (ef) vs nonevaporative terms (ne) for (a) 20, (b) 24, and (c) 25 Jun 2006. Contour lines represent the conceptual model by EH04. for the relative humidity tendency normalized by the $(Q^* - G)$ factor at the rhs of Eq. (1).

$$c_1 = \frac{L_v}{R_v}\frac{q_{\text{sat}}}{T^2}\left(\frac{p}{p_s}\right)^{R_d/c_p} \tag{4}$$

and

$$c_2 = \left(\frac{L_v}{R_v}\frac{q_{\text{sat}}}{T^2} - \frac{c_p}{R_d}\frac{q_{\text{sat}}}{T}\right)\frac{g}{c_p}. \tag{5}$$

Herein R_d and R_v are the gas constant for dry air and water vapor, respectively, and p and p_s the pressure and surface pressure. Also T is the absolute temperature, g the acceleration of gravity, and q_{sat} the saturated specific humidity.

The above conceptual modeling framework results in different regimes (see Fig. 1). First, for ne ≤ 0, a regime can be identified in with $\partial \text{RH}_{\text{top}}/\partial t < 0$. This regime corresponds to findings of EH04 that cloud cover decreases as w is decreased below its wilting point. In the second regime with $0 <$ ne < 1, and $\partial \text{RH}_{\text{top}}/\partial t > 0$, the RH tendency increases for larger w; that is, cloud cover would increase as the soil becomes moister. In the third regime, with ne > 1 and $\partial \text{RH}_{\text{top}}/\partial t < 0$, the RH tendency increases for a decreasing ef. In other words, this is the DSRHI regime where decreasing w would support cumulus onset.

Evaluation of the modeling framework against Cabauw tower observations (the Netherlands) brought forward that ef remains relatively constant throughout the day, whereas ne increases for an evolving ABL. However, for this case at Cabauw, the observations did not enter the DSRHI regime. This means that either γ_θ is rather strong

TABLE 1. Variables and values prescribed to WRF SCM (van Heerwaarden et al. 2010).

Description	Variable (unit)	Value
Surface pressure	P_{surf} (Pa)	98 500
Soil temperature	T_{soil} (K)	300
Temperature of deeper soil	T_{2soil} (K)	290
Albedo	α (−)	0.21
Initial boundary layer depth	$PBLH_i$ (m)	400
Initial mixed-layer potential temperature	θ (K)	301.2
Initial temperature jump at ABL top	$\Delta\theta$ (K)	3.6
Temperature lapse rate	γ_θ (K m^{-1})	0.010 ($z < 700$ m), 0.0034 ($z > 700$ m)
Initial mixed-layer specific humidity	q (kg kg^{-1})	0.0138
Initial specific humidity jump at ABL top	Δq (kg kg^{-1})	−0.0044
Specific humidity lapse rate	γ_q (kg kg^{-1} m^{-1})	-1.4×10^{-6}
Soil moisture content ($0 < d < 0.70$ m)	w (m^3 m^{-3})	0.20
Deep soil moisture content ($d > 0.70$ m)	w (m^3 m^{-3})	0.19

or the free atmospheric air is relatively dry. Similar behavior appeared for the Hydrological Atmospheric Pilot Experiment–Modelisation du Bilan Hydrique (HAPEX–MOBILHY) campaign (southwest France, summer 1986, EH04). Using this framework, we are in search of observational evidence for the DSRHI regime in the AMMA data that are expected to be ideal.

3. Methods

a. Numerical modeling framework

The WRF single-column model (Michalakes et al. 2005; Skamarock et al. 2008) is used to simulate 22 June 2006 during AMMA. Here the ABL schemes MRF (Troen and Mahrt 1986; Holtslag and Boville 1993; Hong and Pan 1996), YSU (Noh et al. 2003; Hong et al. 2006), QNSE (Sukoriansky et al. 2006), and MYJ (Janjíc 2002) are utilized. In short, MRF is based on a nonlocal first-order mixing scheme in the convective ABL. Herein, the turbulent diffusion coefficient has a predefined cubic shape as function of nondimensional height z/h, and its magnitude depends on the velocity scale and surface-layer stability. Furthermore, h is estimated using a critical Richardson number approach (Hong and Pan 1996; Santanello et al. 2009, hereafter S09).

The YSU scheme extends MRF because it explicitly represents ABL top entrainment and countergradient momentum fluxes. MRF is known to overestimate ABL depth and entrainment (e.g., Vogelezang and Holtslag 1996; Dudhia 2002). The YSU scheme alleviates some of these problems and seems to provide more realistic vertical profiles within and above the ABL (Dudhia 2004; Hong et al. 2006; Hu et al. 2010). The Quasi-Normal Scale Elimination and Mellor–Yamada–Janjić schemes are both local turbulent kinetic energy (TKE)-based schemes in which counter gradient transport is absent. QNSE and MYJ differ in their formulation of the length scale and stability dependence of the exchange coefficients. QNSE has been especially designed to account for anisotropy and for momentum transport by waves in the nocturnal ABL. Furthermore, the Noah land surface model has been used for all runs (Ek et al. 2003).

The choice of the LSM and ABL schemes is important since S09 found a greater sensitivity of ef with the choice of the Noah LSM compared to the Community Land Model LSM. S09 found that the Noah scheme generally provides a realistic daily cycle of θ and q. However, the LSM hardly influences the ABL evolution itself. The ABL height varies more significantly between ABL schemes than for different LSMs, particularly for drier soils. This ABL evolution is best simulated by YSU in the considered environment (S09). Thus, we expect the best results from runs using Noah and YSU schemes.

The initial profiles of temperature and humidity for the model simulations have been inspired on the observed sounding taken in Niamey 22 June 2006 at 0835 UTC (van Heerwaarden et al. 2010, Table 1). Soil moisture and temperature are initialized from field observations and have been fine tuned to obtain a close agreement with the observed Bowen ratio, and it appears the model results are very sensitive to the initial soil conditions. Model output is discussed in the context of the EH04 framework.

b. Site description

The Sahel is a subdesert area enclosed by the Sahara desert to the north and the African subtropical areas to the south. Its vegetation consists of sparse grasslands, savannas, and steppes, and its climate is characterized by a dry season November–February and a wet season in March–October. The latter is caused by the intertropical convergence zone (ITCZ), which reaches its

northernmost position in August, coinciding with the most intense precipitation. In June (i.e., the period we will study in this paper), the ITCZ is located over Nigeria (just south of Niger).

In semiarid regions as the Sahel, at first sight, the low surface moisture w acts to limit cumulus onset, but due to the relatively deep ABLs and relatively large Δq, it is therefore hypothesized that atmospheric forcings also play a large role in this region. Hence, the AMMA site in Niamey (time zone UTC +1 h) is ideal for evaluating our model framework. In principle, the same applies to any semiarid region in the world, provided that evaporation is low and the land–atmosphere coupling must be strong.

In semiarid regions, as the U. S. Southern Great Plains (SGP), anthropogenic interference due to agricultural irrigation has increased rainfall and evaporation drastically (Barnston and Schickedanz 1984; Moore and Rojstaczer 2001). Therefore, these regions are not suitable for this research, as LE should be minimal to enter the DSRHI regime. In the Sahel irrigation is less extensive so that natural evaporation is small. Also, the Sahel is a hotspot for land–atmosphere coupling: that is, the soil moisture anomalies have a large impact on ABL evolution and precipitation (Koster et al. 2004).

c. Synoptic situation

The utilized observations have been gathered between 20 and 25 June at the AMMA site of Niamey International Airport, Niger (13.477°N, 2.175°E, 225 m above mean sea level). This episode is at the early stage of the monsoon, and the soil moisture content is still near its wilting point then, inducing the relatively small LE required to answer our research question.

Next, we provide a brief day-by-day description of the synoptic situation: 20 June 2006 was a clear-sky and relatively hot day, with temperatures of 27.2°C in the early morning (0733 UTC) and 34.7°C in the late afternoon (1335 UTC). At the surface the wind was southeasterly and veered to the southwest during the day. At higher altitudes the wind was northeasterly.

In the night preceding 22 June 2006, a MCS provided ~5 mm of rain, of which a large part was already removed via runoff, drainage, or evaporation during the night. Afterward, a clear-sky day started, with a large diurnal cycle of temperature combined with a strong drying of the soil throughout the day. In addition, in the morning, between 0800 and 1100 UTC, advection moistened the atmosphere by about 0.2 g kg^{-1}, while advection vanished in the afternoon (van Heerwaarden et al. 2010). The temperature increased from 28.3°C in the morning (0835 UTC) to a maximum of 37.2°C at 1435 UTC.

The synopsis of 24 June 2006 was slightly different. The day started clear, but a layer of shallow cumulus clouds developed over the area during the morning, which vanished in the afternoon. Temperatures increased from 29.6°C in the morning (0835 UTC) to 37.2°C in the late afternoon (1735 UTC).

The weather on 25 June 2006 did not differ much from 22 June 2006. During the nocturnal hours of 25 June 2006, a MCS developed near Niamey and caused light rainfall. Daylight started as with a clear sky and, owing to the light precipitation, evaporation was relatively strong. In the course of the morning, a strong drying occurred. Temperatures at the surface increased from 28.4°C in the early morning (0833 UTC) to 40.2°C in the afternoon (1433 UTC) and decreased after.

d. Available observations

A key constraint to our research is the need of radio soundings during the daytime ABL development, preferably on a 1–2-h basis (Nuret et al. 2008). The sounding data include temperature, RH, wind speed, and direction. The soundings have been launched every 3 h—four overnight and four during the day. In this study, only the daytime soundings are used, since the framework only applies to the unstable ABL, and we are only interested in the cumulus onset at daytime.

The micrometeorological observations originate from the Atmospheric Radiation Measurement (ARM) Program mobile facility set up at the AMMA measurement site, just outside Niamey Airport. These data include H and LE, air temperature at two meters, incoming and outgoing shortwave radiation, incoming and outgoing longwave radiation, and net radiation. Unfortunately, soil heat flux (G) was not directly measured and a semiempirical approach is required to estimate this quantity. Durand et al. (1988) studied the surface energy budget for the same region in the Sahel, though for the dry period between November 15 and 10 December 1980. They diagnosed G to be ~44% of the net radiation, while Stull (1988) estimates G as 5%–15% of Q^*. Kakane (2004) found typically $G/Q^* \sim 0.22$–0.27 for the greater Accra region, while Goutorbe et al. (1997) observed $G/Q^* = 0.13$–0.21 for HAPEX–Sahel. Inspired by the latter study, we estimate $G = 0.21Q^*$.

To estimate the observed ef, it is essential that the observed surface energy balance is closed. Since the observed energy balance does not close based on the "raw" eddy covariance flux data, we use the hourly based Bowen ratio (β) method to close the surface energy budget:

$$\beta = \frac{H_{\text{raw}}}{LE_{\text{raw}}}. \tag{6}$$

Next, H and LE are estimated by

$$H = \frac{Q^* - G}{(1 + 1/\beta)}, \tag{7}$$

and

$$LE = \frac{Q^* - G}{(1 + \beta)}. \tag{8}$$

Application of this correction resulted in a maximum change of 12% and 26% of LE and H, respectively.

Finally, we filter our observations for sufficient ABL instability, as the conceptual framework is only valid $-h/L > 5$, with L the Obukhov length. Earlier studies have shown that $-h/L > 5$ is sufficient to drive the ABL into the convective state (Deardorff 1974; Holtslag and Nieuwstadt 1986).

4. Results

In this section, we first discuss the AMMA observations of 20, 24, and 25 June in the EH04 framework. Later on, we summarize observational and model results for 22 June.

a. Observations

Figure 1 shows the estimated values of the RH_{top} tendency for the selected days. Considering the meteorological history, 20 June 2006 is a clear day after a dry period. The H is large and LE is negligibly small, thus ef is very small and remains rather constant between 0.15 and 0.20 throughout the day (Fig. 1a). During that day, ne increases with time, from −1.69 at 0733 UTC to 1.60 in the afternoon. As such, the observations confirm the regime ne > 1, as suggested by the EH04 modeling framework. For comparison, in EH04 ne increases from −2.2 to slightly less than 1 for a clear spring day at Cabauw. Thus, the ne increase over the day is comparable for Cabauw and the current AMMA data.

To quantify the robustness of our findings for ne > 1, an uncertainty analysis is required. Vertical error bars in Fig. 1 have been estimated by simultaneously varying the estimated h by 100 m and the estimated Δq at the ABL top by 0.5 g kg^{-1}. Both variables are shown to have the largest impact on estimates of ne. Clearly, the uncertainties are not symmetric around the observed mean value and are larger for smaller ne. Horizontal error bars have been estimated by assuming a ~10% uncertainty of the turbulent surface fluxes. Despite the relatively large uncertainties, the upper point is well above ne = 1, which provides further confidence in our findings.

In addition, a sensitivity analysis on the robustness of the results on the assumed value of C_θ has been performed by varying the original C_θ of 0.2 between 0.1 and 0.3, that is, a 50% change. It appears that for all days the maximum deviation in ne did not exceed 12.5% from its original value, and this has been decisive for only single data point to exceed the threshold value of ne = 1.

For 24 June 2006 Fig. 1b indicates that ef remains again approximately constant and closely ~0.1. Between 0834 and 1135 UTC, ne increases, but this increase is smaller than for 20 June. However, in the 1431 UTC sounding, $\partial RH_{top}/\partial t$ vanishes and ne suddenly drops again, which is unexpected and investigated further. The atmospheric profiles (Fig. 2) during 24 June indicate an increasing q and conditionally unstable layer between ~1200 and 1500 m at 1135 UTC, which suggests the presence of clouds. Satellite observations confirm a shallow cumulus layer at 1130 UTC, though at 1431 UTC the sky was cloud free.

As the conceptual framework only applies for clear-sky conditions, the case of 24 June should, at first sight, be excluded from our analysis. The cloud cover at 1135 UTC reduces the ABL growth, which makes it more plausible for ne to decrease when the clouds are present than to occur after the clouds have dissipated (i.e., at 1431 UTC). It is thus tempting to further study the physical process that forced the cloud dissipation. Observed wind directions reveal a southerly wind in the lower layers, advecting relatively cold and moist air with ~−0.8 K h^{-1} and 0.3 g kg^{-1} h^{-1} from the Nigerian tropical forest. At higher levels, the wind is northeasterly between 1135 and 1431 UTC, and advects relatively dry and warm air that originates from the Sahara. Probably, the clouds have been transported southwestward or evaporated in this dry air above the ABL (as was analyzed from satellite images). Under any circumstances the dry air advection increased Δq, which consequently decreased ne. This dims the probability of cumulus onset.

Compared to the previous cases, ef is relatively high (0.22) in the morning of 25 June and decreases quite sharply during the day (Fig. 1c). The relatively high ef in the morning originates from ~2 mm precipitation after the passage of a MCS during the previous night. Consistent with the previous cases, ne increases rapidly from −0.2 to 2.8 as ef reached nearly the wilting point ($w < 0.171$ m^3 m^{-3}). This indicates that evaporation becomes so small that only atmospheric forcings govern ABL growth and $\partial RH_{top}/\partial t$, which confirms the DSRHI regime.

b. WRF SCM results

To validate WRF single column model, components of the surface energy and radiation balance are evaluated first. Both YSU and MRF follow the observed course of H relatively well, with a positive bias of about 40–60 W m^{-2} after noon (Fig. 3). The latent heat flux

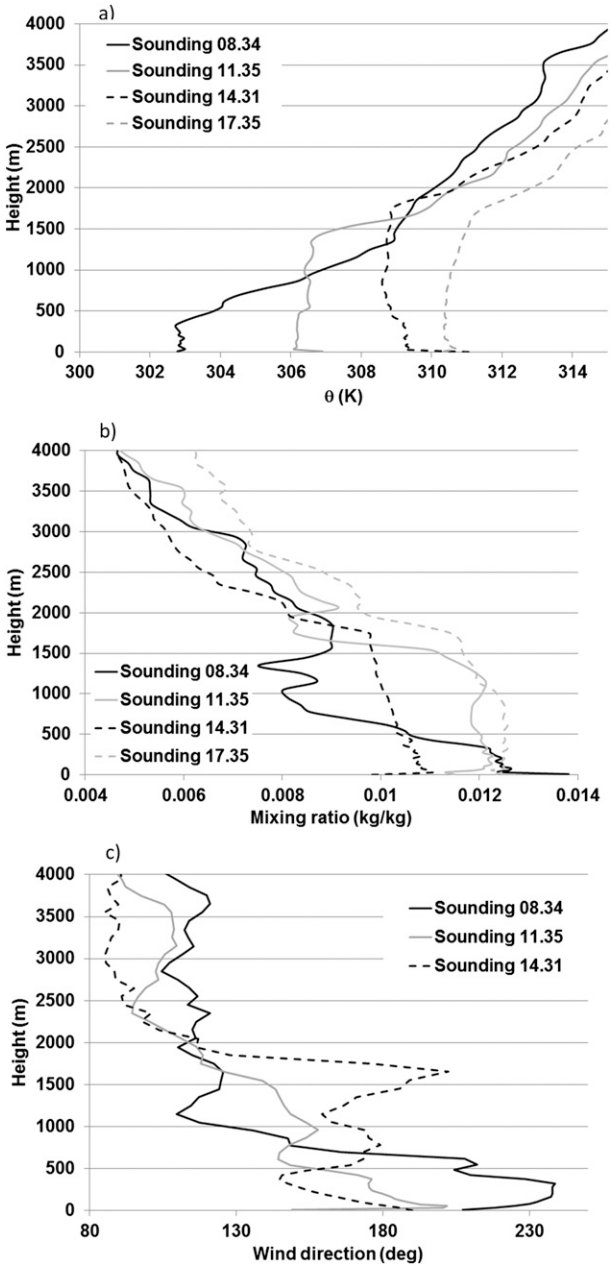

FIG. 2. (a) Observed potential temperature, (b) mixing ratio, and (c) wind direction profiles for 24 Jun 2006.

is forecasted reasonably, until noon, whereafter it is slightly overestimated. MYJ and QNSE forecast H and LE slightly larger than MRF and YSU. Particularly, the H by QNSE is ~60 W m^{-2} larger than in the other runs. That H and LE by MYJ and QNSE are larger than in MRF and YSU is in agreement with the strong near-surface instability close to the surface in the first two models (Fig. 4). In addition, the overestimation of the modeled H and LE suggests that heat exchange with the soil is underestimated by the model or that the ratio of the soil heat flux over net radiation is larger in reality than was assumed in our analysis of the surface energy budget (cf. section 3e). Finally, the modeled LE has a substantial time delay of 1–2 h compared to the observations, which suggests that the soil moisture is depleted more quickly in reality than in the model.

For our study, it is more important for the models to match β and ef rather than to forecast the fluxes precisely. The modeled β is 2.2, whereas the observed β amounts to 2.08. Despite the slight deviation between both values, the model appears to be able to estimate fluxes and β sufficiently to further calculate ef and ne. Although MYJ and QNSE overestimate the surface fluxes, β amounts to 2.3, which is relatively close to the observations and to the other model runs.

Second, we evaluate θ and q profiles, which provisionally indicate whether WRF SCM provides a mixed layer for 22 June (Fig. 4a). The modeled ABL by YSU is initially slightly too warm; however, the bias is small (0.5 K). The modeled profiles of 1133 and 1451 UTC, however, show quite a large deviation from the observed soundings. This holds especially for the θ profile at 1133 UTC and all q profiles. Despite the bias, θ profiles at 1451 and 1740 UTC show better simulation of a mixed layer. The ABL height, however, is overestimated due to relatively strong top entrainment, which is also seen in the specific humidity profiles. Similar results appear with MRF, although its ABL height is even more overestimated than with YSU (Fig. 4b). The modeled profiles using MYJ and QNSE are consistent and are characterized by less well-mixed θ profiles and with a less deep, more humid ABL (Figs. 4c,d) than with YSU or MRF. However, the ABL height and potential temperature θ are relatively well forecasted, in particular at the end of the day. Also, based on the q profiles, the entrainment zone is thinner in MYJ and QNSE compared to YSU and MRF. With QNSE the ABL depth is a number of hundred meters deeper than with MYJ, which results in a stronger entrainment of warm and dry free atmospheric air (in this case).

Applying the EH04 framework to both observations and model runs for 22 June (Fig. 5), we find that the observed ef starts at a relatively large value of 0.46 and shows a sharp decrease to 0.19 at 1451 UTC. This phenomenon is explained by the reduced evaporation after noon, which was initially relatively high owing to the increased soil moisture availability after the mesoscale convective system passage in the previous night. However, the soil apparently rapidly dries out during the first half of the day. All schemes keep ef quite constant at ~0.3 throughout the day with a slight increase to ~0.4 at 1451 UTC. The models forecast ne correctly at 0835 UTC (considering the observational uncertainty).

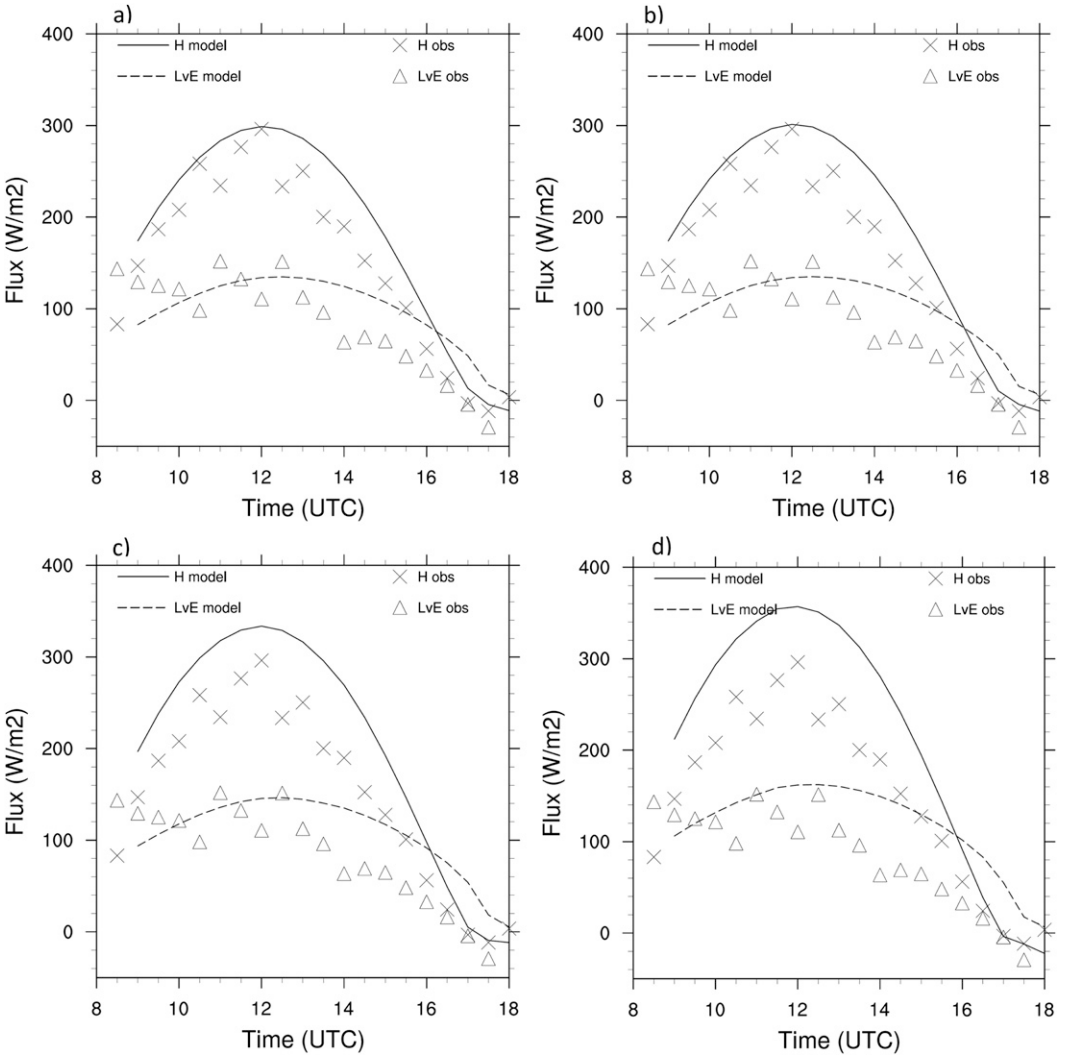

FIG. 3. Observed (symbols) and modeled (solid line) surface fluxes of sensible (H) and latent heat (LE) for 22 Jun 2006; model results for (a) YSU, (b) MRF, (c) MYJ, and (d) QNSE.

At 1133 UTC, ne more rapidly increases in the model runs than in the observations.

In the afternoon, at 1451 UTC, the modeled and observed ne correspond reasonably well between 0.21 by YSU and 2.2 by MRF, while the observed ne equals ~1. As such, the model spread clearly increases in time. However, the observations indicate more dry conditions (smaller ef) than compared to any model run. Prominent here is the difference in the YSU and MRF model output for the value of ne. MRF estimates a much larger ne than YSU or the observations, which can be explained by the deeper ABL in MRF, despite the larger magnitude of Δq in at the ABL top. In addition, the modeled rapid ABL growth enforces the ABL top reaching an area where γ_θ is smaller than in the model runs with other ABL schemes. Moreover, MRF reaches the largest RH_{top} of all simulations, that is, 0.65. As such, the first two terms within brackets in Eq. (3) seem dominating in the MRF simulation. MYJ produces the second largest ne, a result of its relatively shallow ABL. However, a more detailed analysis indicated that for MYJ none of the three terms dominate compared to the other models, but it is the combinations of the magnitudes of the three terms that allow for a relatively large ne.

Note that a more elaborated model evaluation—for example, an evaluation of the trajectory of each model in the (ef, ne) space—would probably provide a deeper understanding of the model deficiencies. However, a more extensive observational dataset would be required to perform such an analysis, and this remains open for future work.

Finally, it is important to discuss the fact that we neglected the role of both temperature and moisture

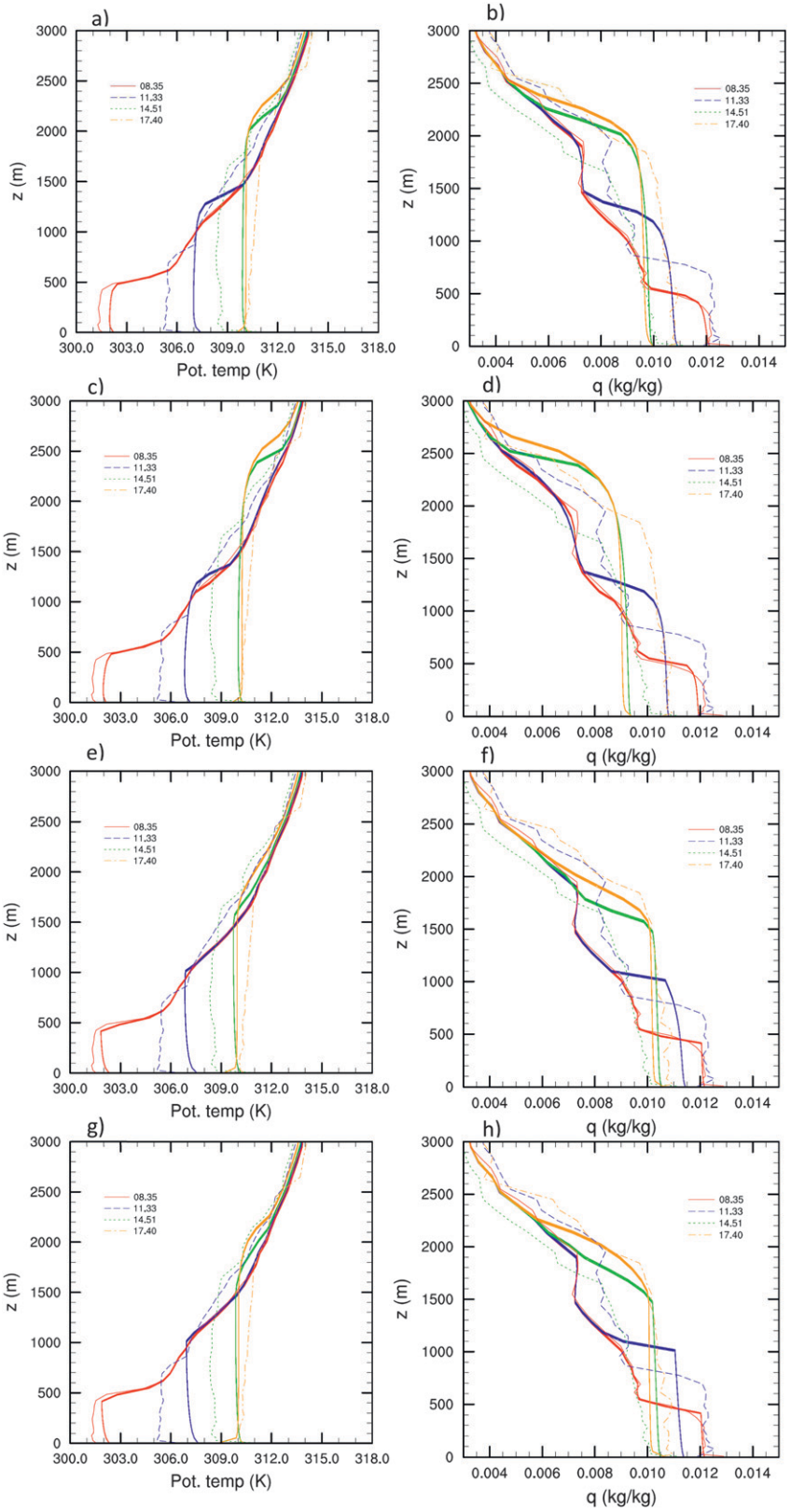

FIG. 4. Modeled (solid lines) and observed (dashed line) (left) potential temperature and (right) mixing ratio for (a),(b) YSU, (c),(d) MRF, (e),(f) MYJ, and (g),(h) QNSE on 22 Jun 2006.

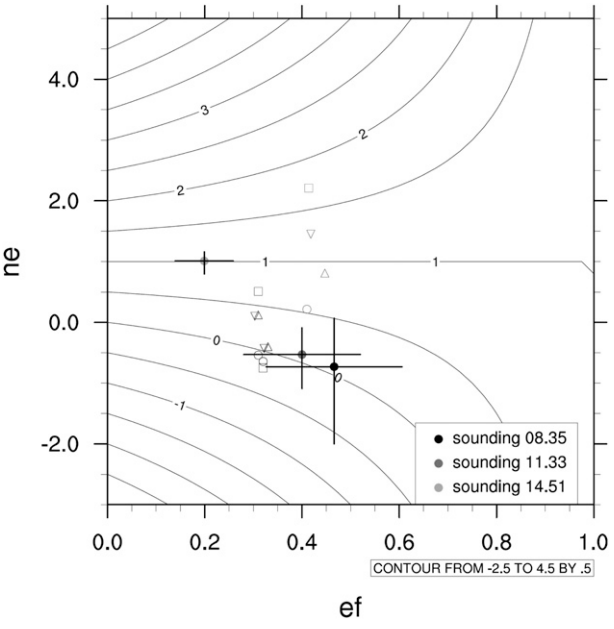

FIG. 5. The normalized RH_{top} tendency as a function of evaporative fraction (ef) vs nonevaporative terms (ne). Contour lines represent the conceptual model by EH04. Observations (●) and model output for the YSU (○), MRF (□), QNSE (Δ), and MYJ (∇) boundary layer schemes for 22 Jun 2006.

advection in this study. The quantitative contribution of moisture advection is relatively small because moisture advection is dominant in the early morning before our model simulations start (as in van Heerwaarden et al. 2010). Temperature advection is most prominent in the period 0800–1100 UTC and amounts to -0.3 K h^{-1} at maximum. Estimating the impact of temperature advection on $\partial RH/\partial t$, we consider that

$$\frac{\partial \mathrm{RH}}{\partial t} = \frac{\partial}{\partial t}\left(\frac{q}{q_{\mathrm{sat}}}\right) = \frac{-q}{q_{\mathrm{sat}}^2}\frac{\partial q_{\mathrm{sat}}}{\partial t} = \frac{-q}{q_{\mathrm{sat}}^2}\frac{dq_{\mathrm{sat}}}{dT}\frac{\partial T}{\partial t}. \quad (9)$$

For the typical cases at hand in our study with $q = 0.010$ kg kg^{-1}, $q_{\mathrm{sat}} = 0.017$ kg kg^{-1}, $dq_{\mathrm{sat}}/dT = 0.0009$ K^{-1}, and $\partial T/\partial t = -0.3$ K h^{-1} $= -8.3 \times 10^{-5}$ K s^{-1}. Then $\partial RH/\partial t = 2.5 \times 10^{-6}$ s^{-1}, which may result in a RH change of 3.7% during the morning from 0800 to 1100 UTC. After 1100 UTC advection is substantially smaller and even positive at higher levels in the ABL. Overall, the analysis indicates that the contribution by advection has been relatively small.

5. Conclusions

This study utilizes AMMA field observations in the Sahel region (Niamey, Niger) to find observational evidence for dry soils supporting enhanced relative humidity at the boundary layer top. The latter would support low-level cumulus cloud formation. Until now, this regime has only been suggested by a conceptual framework formulated in terms of evaporative fraction (ef) and nonevaporative terms (ne). The AMMA observations are particularly suitable for evaluating this regime because of its relatively deep boundary layers, its relatively weak free atmospheric stratification, its relatively low soil moisture, and availability of radio soundings during the ABL evolution. The observations confirm the hypothesis of EH04 for two of the four days studied (i.e., 20 and 25 June 2006). For June 20 and 25, observations in the regime ne $>$ 1 are found, as required to confirm the aforementioned regime. For 24 June, the hypothesis cannot be confirmed, as a shallow layer of cumulus clouds occurred in the morning hours. On 22 June, the observations approached the regime ne $\cong$ 1, but did not substantially exceed the threshold value.

The present study covers only a relatively small dataset and future confirmation by other data is recommended. However, it requires specifically targeted experimental design since all observations from different platforms need to be available simultaneously. Such an experiment, preferably over sites with relative small soil moisture content, should cover radio soundings launched with high frequency (preferably hourly), and simultaneous observations of all components of the surface radiation and energy balance as well as soil moisture availability.

In this paper, we also evaluate the WRF single-column model for 22 June 2006 using various ABL schemes. Overall, the model underestimates the inversion strength, while the free atmospheric stability is well estimated, and the turbulent surface fluxes are overestimated. Considering the modeled $\partial RH_{top}/\partial t$ as a function of ef versus ne, the model does not follow the observations. The model underestimates ef in the morning and overestimates ef in the afternoon. Typically, the model's main limitation is its overestimation of both latent and sensible heat flux after noon. On the other hand, the atmospheric forcings and ne are simulated rather well, but differ substantially between the selected boundary layer schemes. MRF overestimates ne, particularly because the model overestimates the entrainment and therefore produces a relatively large humidity discontinuity, and thus atmospheric forcings are dominant. Overall, the boundary layer schemes utilized remain to have difficulty with cases as studied in this paper. However, future ABL model improvement for the subject studied here would rely on the availability of observations of the full trajectory in the (ef, ne) space.

Acknowledgments. The authors acknowledge F. Couvreux, F. Guichard (CNRM), C. C. van Heerwaarden, and J. Vilà-Guerau de Arellano (Wageningen University)

for providing background information and data. Furthermore, we thank the AMMA program for gathering, quality controlling, and providing the data for the current research. Based on a French initiative, AMMA was developed by an international scientific group and funded by a large number of agencies, especially from Africa, the European community, France, the United Kingdom, and the United States. More information on the scientific coordination and funding is available on the AMMA International website: http://www.amma-international.org. Finally, we also thank three anonymous reviewers for their valuable and constructive comments on the manuscript.

REFERENCES

Barnston, A. G., and P. T. Schickedanz, 1984: The effect of irrigation on warm season precipitation in the southern Great Plains. *J. Climate Appl. Meteor.,* **23,** 865–888.

Bechtold, P., J. P. Chaboureau, A. Beljaars, A. K. Betts, M. Köhler, M. Miller, and J. L. Redelsperger, 2004: The simulation of the diurnal cycle of convective precipitation over land in a global model. *Quart. J. Roy. Meteor. Soc.,* **130,** 3119–3137.

Betts, A. K., and C. Jakob, 2002: Study of diurnal cycle of convective precipitation over Amazonia using a single column model. *J. Geophys. Res.,* **107,** 4732, doi:10.1029/2002JD002264.

Comer, R. E., A. Slingo, and R. P. Allan, 2007: Observations of the diurnal cycle of outgoing longwave radiation from the Geostationary Earth Radiation Budget instrument. *Geophys. Res. Lett.,* **34,** L02823, doi:10.1029/2006GL028229.

Couvreux, F., C. Rio, F. Guichard, M. Lothon, G. Canut, D. Bouniol, and A. Gounou, 2012: Initiation of daytime local convection in a semi-arid region analysed with high-resolution simulations and AMMA observations. *Quart. J. Roy. Meteor. Soc.,* **138,** 56–71.

Deardorff, J. W., 1974: Three-dimensional numerical study of the height and mean structure of a heated planetary boundary layer. *Bound.-Layer Meteor.,* **7,** 81–106.

——, 1979: Prediction of convective mixed-layer entrainment for realistic capping inversion structure. *J. Atmos. Sci.,* **36,** 424–436.

Driedonks, A. G. M., and H. Tennekes, 1984: Entrainment effects in the well-mixed boundary layer. *Bound.-Layer Meteor.,* **30,** 75–105.

Dudhia, J., 2004: The Weather Research and Forecast Model version 2.0: Physics update. Preprints, *Fifth WRF/14th MM5 Users' Workshop,* Boulder, CO, NCAR, 1.1. [Available online at http://www.mmm.ucar.edu/mm5/workshop/ws04/Session1/Dudhia.Jimy2.pdf.]

Durand, P., J. P. Frangi, and A. Druilhet, 1988: Energy budget for the Sahel surface layer during the ECLATS experiment. *Bound.-Layer Meteor.,* **42,** 27–42.

Ek, M., and L. Mahrt, 1994: Daytime evolution of relative humidity at the boundary layer top. *Mon. Wea. Rev.,* **122,** 2709–2721.

——, and A. A. M. Holtslag, 2004: Influence of soil moisture on boundary layer cloud development. *J. Hydrometeor.,* **5,** 86–99.

——, K. E. Mitchell, Y. Lin, E. Rogers, P. Grunmann, V. Koren, G. Gayno, and J. D. Tarpley, 2003: Implementation of the Noah land surface model advances in the National Centers for Environmental Prediction operational mesoscale Eta model. *J. Geophys. Res.,* **108,** 8851, doi:10.1029/2002JD003296.

Goutorbe, J. P., J. Noilhan, P. Lacarrere, and I. Braud, 1997: Modelling of the atmospheric column over the Central sites during HAPEX-Sahel. *J. Hydrol.,* **188–189,** 1017–1039.

Guichard, F., and Coauthors, 2004: Modelling the diurnal cycle of deep precipitating convection over land with cloud-resolving models and single-column models. *Quart. J. Roy. Meteor. Soc.,* **130,** 3139–3172.

Haiden, T., 1997: An analytical study of cumulus onset. *Quart. J. Roy. Meteor. Soc.,* **123,** 1945–1960.

Holtslag, A. A. M., and F. T. M. Nieuwstadt, 1986: Scaling the atmospheric boundary layer. *Bound.-Layer Meteor.,* **36,** 201–209.

——, and B. A. Boville, 1993: Local versus nonlocal boundary-layer diffusion in a global climate model. *J. Climate,* **6,** 1825–1842.

Hong, S. Y., and H. L. Pan, 1996: Nonlocal boundary layer vertical diffusion in a medium-range forecast model. *Mon. Wea. Rev.,* **124,** 2322–2339.

——, Y. Noh, and J. Dudhia, 2006: A new vertical diffusion package with an explicit treatment of entrainment processes. *Mon. Wea. Rev.,* **134,** 2318–2341.

Hu, X. M., J. W. Nielsen-Gammon, and F. Zhang, 2010: Evaluation of three planetary boundary layer schemes in the WRF model. *J. Appl. Meteor. Climatol.,* **49,** 1831–1844.

Jacobs, C. M. J., and H. A. R. De Bruin, 1992: The sensitivity of regional transpiration to land-surface characteristics: Significance of feedback. *J. Climate,* **5,** 683–698.

Janjíc, Z. I., 2002: Nonsingular implementation of the Mellor–Yamada level 2.5 scheme in the NCEP Meso model. NCEP Office Note 437, 61 pp.

Kakane, V. C. K., 2004: Soil heat flux–net radiation relation for some surfaces. *West Afr. J. Appl. Ecol.,* **5,** 21–29.

Koster, R. D., and Coauthors, 2004: Regions of strong coupling between soil moisture and precipitation. *Science,* **305,** 1138–1140.

Lothon, M., B. Campistron, M. Chong, F. Couvreux, F. Guichard, C. Rio, and E. Williams, 2011: Life cycle of a mesoscale circular gust front observed by a C-band Doppler radar in West Africa. *Mon. Wea. Rev.,* **139,** 1370–1388.

Michalakes, J., J. Dudhia, D. Gill, T. Henderson, J. Klemp, W. Skamarock, and W. Wang, 2005: The Weather Research and Forecast model: Software architecture and performance. *Proc. 11th Workshop on the Use of High Performance Computing in Meteorology,* Reading, United Kingdom, ECMWF, 156–168.

Moore, N., and S. Rojstaczer, 2001: Irrigation-induced rainfall and the Great Plains. *J. Appl. Meteor.,* **40,** 1297–1309.

Noh, Y., W. G. Cheon, S. Y. Hong, and S. Raasch, 2003: Improvement of the *K*-profile model for the planetary boundary layer based on large eddy simulation data. *Bound.-Layer Meteor.,* **107,** 401–427.

Nuret, M., J.-P. Lafore, F. Guichard, J.-L. Redelsperger, O. Bock, A. Agusti-Panareda, and J.-B. N'Gamini, 2008: Correction of humidity bias for Vaisala RS80-A sondes during the AMMA 2006 observing period. *J. Atmos. Oceanic Technol.,* **25,** 2152–2158.

Redelsperger, J. L., C. D. Thorncroft, A. Diedhiou, T. Lebel, D. J. Parker, and J. Polcher, 2006: African Monsoon Multidisciplinary Analysis: An international research project and field campaign. *Bull. Amer. Meteor. Soc.,* **87,** 1739–1746.

Rio, C., F. Hourdin, J.-Y. Grandpeix, and J.-P. Lafore, 2009: Shifting the diurnal cycle of parameterized deep convection over land. *Geophys. Res. Lett.,* **36,** L07809, doi:10.1029/2008GL036779.

Santanello J. A., Jr., M. A. Friedl, and W. P. Kustas, 2005: An empirical investigation of convective planetary boundary layer evolution and its relationship with the land surface. *J. Appl. Meteor.,* **44,** 917–932.

——, ——, and M. B. Ek, 2007: Convective planetary boundary layer interactions with the land surface at diurnal time scales: Diagnostics and feedbacks. *J. Hydrometeor.,* **8,** 1082–1097.

——, C. D. Peters-Lidard, S. V. Kumar, C. Alonge, and W. K. Tao, 2009: A modeling and observational framework for diagnosing local land–atmosphere coupling on diurnal time scales. *J. Hydrometeor.,* **10,** 577–599.

Schlemmer, L., O. Martius, M. Sprenger, C. Schwierz, and A. Twitchett, 2010: Disentangling the forcing mechanisms of a heavy precipitation event along the Alpine south side using potential vorticity inversion. *Mon. Wea. Rev.,* **138,** 2336–2353.

——, C. Hohenegger, J. Schmidli, C. S. Bretherton, and C. Schär, 2011: An idealized cloud-resolving framework for the study of midlatitude diurnal convection over land. *J. Atmos. Sci.,* **68,** 1041–1057.

Skamarock, W., and Coauthors, 2008: A description of the Advanced Research WRF version 3. Mesoscale and Microscale Meteorology Division, National Center for Atmospheric Research Tech. Note NCAR/TN–475+STR, 113 pp. [Available online at www.mmm.ucar.edu/wrf/users/docs/arw_v3.pdf.]

Stull, R. B., 1988: *An Introduction to Boundary Layer Meteorology*. Kluwer Academic, 666 pp.

Sukoriansky, S., B. Galperin, and V. Perov, 2006: A quasi-normal scale elimination model of turbulence and its application to stably stratified flow. *Nonlinear Processes Geophys.,* **13,** 9–22.

Taylor, C. M., A. Gounou, F. Guichard, P. P. Harris, R. J. Ellis, F. Couvreux, and M. de Kauwe, 2011: Frequency of Sahelian storm initiation enhanced over mesoscale soil-moisture patterns. *Nat. Geosci.,* **4,** 430–433.

Taylor, N. M., and Coauthors, 2011: The Understanding Severe Thunderstorms and Alberta Boundary Layers Experiment (UNSTABLE) 2008. *Bull. Amer. Meteor. Soc.,* **92,** 739–763.

Troen, I. B., and L. Mahrt, 1986: A simple model of the atmospheric boundary layer: Sensitivity to surface evaporation. *Bound.-Layer Meteor.,* **37,** 129–148.

van Heerwaarden, C. C., J. Vilà-Guerau de Arellano, A. F. Moene, and A. A. M. Holtslag, 2009: Interactions between dry-air entrainment, surface evaporation and convective boundary-layer development. *Quart. J. Roy. Meteor. Soc.,* **135,** 1277–1291.

——, ——, A. Gounou, F. Guichard, and F. Couvreux, 2010: Understanding the daily cycle of evapotranspiration: A method to quantify the influence of forcings and feedbacks. *J. Hydrometeor.,* **11,** 1405–1422.

Vogelezang, D. H. P., and A. A. M. Holtslag, 1996: Evaluation and model impacts of alternative boundary-layer height formulations. *Bound.-Layer Meteor.,* **81,** 245–269.

Wetzel, P. J., 1990: A simple parcel method for prediction of cumulus onset and area-averaged cloud amount over heterogeneous land surfaces. *J. Appl. Meteor.,* **29,** 516–523.

Wilde, N. P., R. B. Stull, and E. W. Eloranta, 1985: The LCL zone and cumulus onset. *J. Climate Appl. Meteor.,* **24,** 640–657.